

On the shape of the spectrum of cosmic-rays accelerated inside superbubbles

Gilles Ferrand¹ and Alexandre Marcowith²

¹ Institut de recherche sur les lois fondamentales de l'Univers (Irfu), Service d'Astrophysique (SAp)
Orme des Merisiers, CEA Saclay, 91191 Gif-sur-Yvette Cedex, France
e-mail: g.ferrand@cea.fr

² Laboratoire de Physique Théorique et Astroparticules (LPTA), CNRS, Université Montpellier II
Place Eugène Bataillon, 34095 Montpellier Cédex, France
e-mail: alexandre.marcowith@lpta.in2p3.fr

2009/10/21

ABSTRACT

Context. Supernova remnants are believed to be a major source of energetic particles (*cosmic-rays*) at the Galactic scale. As their progenitors, namely the most massive stars, are commonly found clustered in *OB associations*, one has to consider the possibility of collective effects in the acceleration process.

Aims. In this work we investigate the shape of the spectrum of high-energy protons produced inside the *superbubbles* blown around clusters of massive stars.

Methods. To do so we embed simple semi-analytical models of particle acceleration and transport inside Monte-Carlo simulations of OB associations timelines. We consider regular acceleration (Fermi 1 process) at the shock front of supernova remnants, as well as stochastic re-acceleration (Fermi 2 process) and escape (controlled by magnetic turbulence) occurring between the shocks. In this first attempt we limit ourselves to linear acceleration by strong shocks and neglect protons energy losses.

Results. We observe that particle spectra, although strongly intermittent, get a distinctive shape resulting from a competition between acceleration and escape: they are harder at the lowest energies (index $s < 4$) and softer at the highest energies ($s > 4$). The momentum at which this spectral break occurs depends on the various bubble parameters, but all their effects can be summarized by a single dimensionless parameter, which we evaluate for a selection of massive stars regions in the Galaxy and in the LMC.

Conclusions. The behaviour of a superbubble regarding particle acceleration critically depends on the magnetic turbulence: if B is low then the superbubble is simply the host of a collection of individual supernovae shocks, but if B is high enough (and the turbulence index is not too high), then the superbubble acts as a global accelerator, producing distinctive spectra, potentially very hard over a large range of energies – which has important implications on the high-energy emission from these objects.

Key words. acceleration of particles – shock waves – turbulence – cosmic rays – supernova remnants

1. Introduction

Superbubbles are hot and tenuous large structures formed around OB associations by the powerful winds and by the explosions of massive stars (Higdon & Lingenfelter 2005). They are the major hosts of supernovae in the Galaxy, and thus major candidates for the production of energetic particles (eg Montmerle 1979, Bykov 2001, Butt 2009, and references therein). Supernovae are indeed believed to be the main contributors of Galactic cosmic-rays (along with pulsars and micro-quasars), through the *diffusive shock acceleration* process (a 1st-order, regular Fermi process) taking place at the remnant's blast wave as it goes through the interstellar medium (Drury 1983; Malkov & Drury 2001).

Supernovae in superbubbles are correlated in space and time, hence the need to investigate acceleration by multiple shocks (Parizot et al. 2004). Klepach et al. (2000) have developed a semi-analytical model of test-particle acceleration by multiple spherical shocks (either winds termination shocks, either supernova shocks and winds external shocks), under the limiting assumption of small shocks filling factors. Ferrand et al. (2008) have made direct numerical simulations of repeated acceleration by successive planar shocks in the non-linear regime (that is, taking into account the back-reaction of energetic particles on the flow). But in order to work out the particles spectrum produced

inside the superbubble as a whole, one has to consider also important physics occurring *between* the shocks: as the bubble interior is likely magnetized and turbulent, we need to evaluate gains and losses due to acceleration by waves (a 2nd-order, stochastic Fermi process) and escape from the bubble.

In this study, we combine the effects of regular acceleration (occurring quite discreetly, at shock fronts) and stochastic acceleration and escape (occurring continuously, between shocks), in order to work out the typical spectra that we can expect inside superbubbles over the lifetime of an OB cluster. We choose to treat regular acceleration as simply as we can, and concentrate on modeling the relevant scales of stochastic acceleration and escape inside superbubbles. We present our model in section 2, give our general results in section 3 and present specific applications in section 4. Finally we discuss the limitations of our approach in section 5 and give our conclusions in section 6.

2. Model

Our model is based on Monte-Carlo simulations of the activity of a cluster of massive stars, in which we embed simple semi-analytical models of (re-)acceleration and escape (described through their Green functions). In order to work out the average

properties of a cluster of N_\star stars, we perform random samplings in the Initial Mass Function (Sec. 2.1). For a given cluster, time is sampled by intervals $dt = 10\,000$ yr, which is small enough to make sure that at most one supernova occurs during that period – but by chance for big clusters, and which is big enough to consider that regular acceleration at a shock front has shaped the spectrum of particles – acceleration is thought to take place mostly at early stages of supernova remnants evolution, and in a superbubble the Sedov phase starts after a few thousands of years (Parizot et al. 2004). Here we do not try to investigate the exact extent of the spectrum of accelerated particles: we set the lowest momentum (injection momentum) to $p_{\min} = 10^{-2} m_p c$ (which is the typical thermal momentum downstream of a supernova shock) and we set the highest momentum (escape momentum) to $p_{\max} = 10^6 m_p c \simeq 10^{15}$ eV (which corresponds to the “knee” break in the spectrum of cosmic-rays as observed on the Earth). Note that the theoretical acceleration time from p_{\min} to p_{\max} (in the linear regime, without escape) is roughly 8 000 yr (assuming Bohm diffusion with $B = 10 \mu G$), which is again consistent with our choice of dt . This makes 8 decades in p , with a resolution of a few tens of bins per decade (according to Sec. 2.2.2).

The procedure is then as follows: for each time bin in the life of the cluster, either a supernova occurs, and the distribution of particles is modified according to the diffusive shock acceleration process, as explained in Sec. 2.2; either no supernova occurs, and the distribution is evolved in time taking into account acceleration and escape through interaction with magnetic turbulence, as explained in Sec. 2.3. This process is repeated for many random clusters of the same size, until some average trend emerges regarding the shape of spectra (note that average spectra are not monitored for each bin dt but by larger steps of 1 Myr).

In the following we detail our description of massive stars, supernovae shocks, and magnetic turbulence.

2.1. OB clusters: random samplings of supernovae

We are interested here in massive stars which die by core-collapse, producing type Ib, Ic or II supernovae, that is of mass greater than $m_{\min} = 8 m_\odot$, and up to say $m_{\max} = 120 m_\odot$. These are stars of spectral type O ($> 20 m_\odot$) and part of stars of spectral type B ($4 - 20 m_\odot$). Most massive stars spend all their life within the cluster in which they were born, forming OB associations. In order to describe the evolution of such a cluster, one needs to know the distribution of star masses and lifetimes.

The Initial Mass Function (IMF) ξ is defined so that the number of stars in the mass interval m to $m + dm$ is $dn = \xi(m) \times dm$, so that the number of stars of masses between m_{\min} and m_{\max} is $N_\star = \int_{m_{\min}}^{m_{\max}} \xi(m) dm$. Observations show that ξ can be expressed as a power-law (Salpeter 1955):

$$\xi(m) \propto m^\alpha, \quad (1)$$

with an index of $\alpha = 2.30$ for massive stars (Kroupa 2002). This function is shown in Fig. 1.

Stars lifetimes can be computed from stellar evolution models, we use here data from Limongi & Chieffi (2006), plotted on Fig. 2. The more massive they are, the faster stars burn their material. A star at the threshold $m_{\min} = 8 m_\odot$ has a lifetime of $t_{\text{SN,max}} \simeq 37$ Myr, which is also the total lifetime of the cluster; a star of $m_{\max} = 120 m_\odot$ lives only $t_{\text{SN,min}} \simeq 3$ Myr. Regarding supernovae, the active lifetime of the cluster is thus

$$\Delta t_{\text{OB}}^\star = t_{\text{SN}}(m_{\min}) - t_{\text{SN}}(m_{\max}) \simeq 34 \text{ Myr}. \quad (2)$$

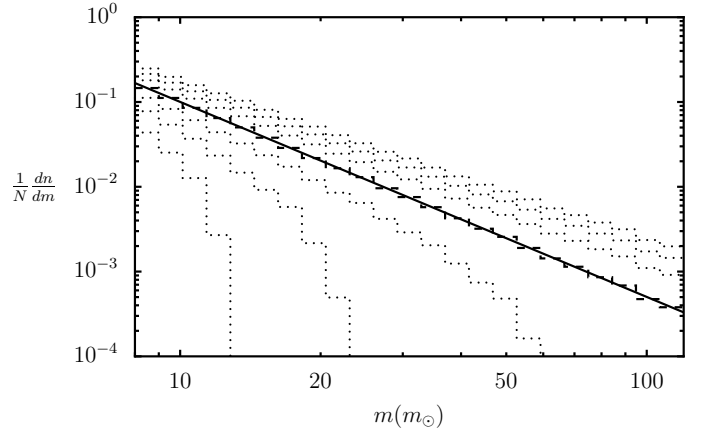


Fig. 1. Distribution of massive stars masses: the Initial Mass Function. For each cluster $N_\star = 100$ stars are randomly chosen in the IMF (1). The dashed curve represents the experimental histogram of masses after $N_{\text{OB}} = 1000$ samples (with resolution $d \log m = 0.05$). The dotted curves show 1-, 2-, 3-sigma standard deviations over the clusters set. The solid curve is the theoretical IMF.

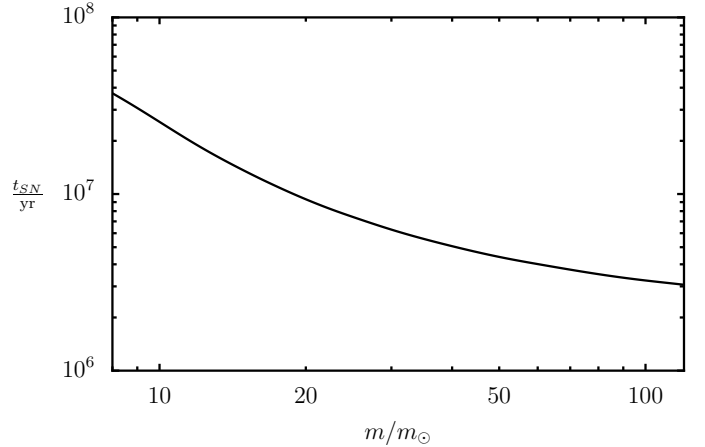


Fig. 2. Distribution of massive stars lifetimes (data from Limongi & Chieffi (2006)).

2.2. Supernovae shocks: regular acceleration

2.2.1. Green function

To keep things as simple as possible, we limit ourselves here to the test-particle approach (non-linear calculations will be presented elsewhere). In the linear regime, we know the Green function G_1 which links the distributions¹ of particles downstream and upstream of a single shock according to

$$f_{\text{down}}(p) = \int_0^\infty G_1(p, p_0) f_{\text{up}}(p_0) dp_0; \quad (3)$$

it reads

$$G_1(p, p_0) = \frac{s_1}{p_0} \left(\frac{p}{p_0} \right)^{-s_1} H(p - p_0) \quad (4)$$

where H is the Heaviside function, and

$$s_1 = \frac{3r}{r-1} \quad (5)$$

¹ The distribution function $f(p)$ is defined so that the particles number density is $n = \int_p f(p) 4\pi p^2 dp$, where p is the momentum.

where r is the compression ratio of the shock.

2.2.2. Adiabatic decompression

Around an OB association, particles produced by a supernova shock might be re-accelerated by the shocks of subsequent supernova before they escape the superbubble. The effect of repeated acceleration is basically to harden the spectra (Achterberg 1990, Melrose & Pope 1993).

When dealing with multiple shocks, it is mandatory to account for adiabatic decompression between the shocks: energetic particles bound to the fluid will see their momenta decreased by a factor $R = r^{1/3}$ when the fluid density is decreased by a factor r . In order to resolve decompression properly, the numerical momentum resolution $d \log p$ has to be significantly smaller than the induced momentum shift (Ferrand et al. 2008).

2.3. Magnetic turbulence: stochastic acceleration and escape

Particles accelerated by supernova shocks, although energetic, might remain for a while inside the superbubble because of magnetic turbulence which scatters them (they perform a random walk until they escape). Because of this turbulence, particles will also experience stochastic re-acceleration during their stay in the bubble. We present here a deliberately simple model of transport, in order to get the relevant functional dependences and order of magnitudes of the diffusion coefficients. The turbulent magnetic field δB is represented through its power spectrum $W(k)$, defined so that $\delta B^2 \propto \int_{k_{\min}}^{k_{\max}} W(k) dk$ with $k = 2\pi/\lambda$ where λ is the turbulence scale. k_{\min} (resp. k_{\max}) corresponds to waves interacting with the particles of highest (resp. lowest) energy. This spectrum is usually taken to be a power-law of index q :

$$W(k) \propto k^{-q}, \quad (6)$$

normalised through the turbulence level

$$\eta_T = \frac{\langle \delta B^2 \rangle}{B^2 + \langle \delta B^2 \rangle}. \quad (7)$$

2.3.1. Diffusion scales

If turbulence follows Eq. (6) then the space diffusion coefficient goes as

$$D_x(p) = D_x^* \times \left(\frac{p}{m_p c} \right)^{2-q} \quad (8)$$

(we assume that the turbulence spectrum extends enough so that this description of D_x remains correct for the lowest particle energies). Using results from Casse et al. (2002) (obtained for isotropic turbulence), one can express

$$D_x^* \propto \eta_T^{-1} B^{q-2} \lambda_{\max}^{q-1}. \quad (9)$$

For standard turbulence indices, we get

$$\frac{D_x(p)}{10^{26} \text{ cm}^2 \cdot \text{s}^{-1}} \simeq \begin{cases} \frac{12.3}{\eta_T} \left(\frac{B}{10 \mu\text{G}} \right)^{-\frac{1}{3}} \left(\frac{\lambda_{\max}}{10 \text{ pc}} \right)^{\frac{2}{3}} \left(\frac{p}{m_p c} \right)^{\frac{1}{3}} & q = 5/3 \\ \frac{0.8}{\eta_T} \left(\frac{B}{10 \mu\text{G}} \right)^{-\frac{1}{2}} \left(\frac{\lambda_{\max}}{10 \text{ pc}} \right)^{\frac{1}{2}} \left(\frac{p}{m_p c} \right)^{\frac{1}{2}} & q = 3/2 \end{cases} \quad (10)$$

Particles diffuse over a typical length $x_{\text{diff}} = \sqrt{6 D_x t}$. They are confined in the acceleration region of size x_{acc} as long as

$x_{\text{diff}}(t) < x_{\text{acc}}$, hence a typical escape time $t_{\text{esc}} = x_{\text{acc}}^2 / 6 D_x$, that is using Eq. (8)

$$t_{\text{esc}}(p) = t_{\text{esc}}^* \times \left(\frac{p}{m_p c} \right)^{q-2} \quad (11)$$

with

$$t_{\text{esc}}^* \propto \eta_T B^{2-q} \lambda_{\max}^{1-q} x_{\text{acc}}^2. \quad (12)$$

For standard turbulence indices, we get

$$\frac{t_{\text{esc}}(p)}{10^{13} \text{ s}} \simeq \begin{cases} \frac{\eta_T}{5.0} \left(\frac{B}{10 \mu\text{G}} \right)^{\frac{1}{3}} \left(\frac{\lambda_{\max}}{10 \text{ pc}} \right)^{-\frac{2}{3}} \left(\frac{x_{\text{acc}}}{40 \text{ pc}} \right)^2 \left(\frac{p}{m_p c} \right)^{-\frac{1}{3}} & q = 5/3 \\ \frac{\eta_T}{0.3} \left(\frac{B}{10 \mu\text{G}} \right)^{\frac{1}{2}} \left(\frac{\lambda_{\max}}{10 \text{ pc}} \right)^{-\frac{1}{2}} \left(\frac{x_{\text{acc}}}{40 \text{ pc}} \right)^2 \left(\frac{p}{m_p c} \right)^{-\frac{1}{2}} & q = 3/2 \end{cases} \quad (13)$$

Interaction with waves also leads to a diffusion in momentum. Using results from quasi-linear theory we can express the diffusion coefficient as

$$D_p(p) = D_p^* \times (m_p c)^2 \times \left(\frac{p}{m_p c} \right)^q \quad (14)$$

with

$$D_p^* \propto \eta_T B^{4-q} \lambda_{\max}^{1-q} n^{-1}. \quad (15)$$

where n is the number density (which comes to play through the Alfvén velocity). For standard turbulence indices, we get

$$\frac{D_p(p)}{10^{-38} \text{ g}^2 \cdot \text{cm}^2 \cdot \text{s}^{-3}} \simeq \begin{cases} \frac{\eta_T}{20} \left(\frac{B}{10 \mu\text{G}} \right)^{\frac{7}{3}} \left(\frac{\lambda_{\max}}{10 \text{ pc}} \right)^{-\frac{2}{3}} \left(\frac{n}{10^{-2} \text{ cm}^{-3}} \right)^{-1} \left(\frac{p}{m_p c} \right)^{\frac{5}{3}} & q = 5/3 \\ \frac{\eta_T}{1.4} \left(\frac{B}{10 \mu\text{G}} \right)^{\frac{5}{2}} \left(\frac{\lambda_{\max}}{10 \text{ pc}} \right)^{-\frac{1}{2}} \left(\frac{n}{10^{-2} \text{ cm}^{-3}} \right)^{-1} \left(\frac{p}{m_p c} \right)^{\frac{3}{2}} & q = 3/2 \end{cases} \quad (16)$$

2.3.2. Green function

Becker et al. (2006) have recently given the first analytical expression of the Green function G_2 for both stochastic acceleration and escape, valid for any turbulence index $q \in]0, 2[$. It is defined so that, for impulsive injection of distribution f_{init} , the distribution after time t is

$$f_{\text{end}}(p, t) = \int_0^\infty G_2(p, p_0, t) f_{\text{init}}(p_0) dp_0. \quad (17)$$

Neglecting losses it can be expressed as

$$G_2(p, p_0, t) = \frac{2-q}{p_0} \sqrt{\frac{p}{p_0}} \frac{\sqrt{zz_0\xi}}{1-\xi} \quad (18)$$

$$\times \exp\left(-\frac{(z+z_0)(1+\xi)}{2(1-\xi)}\right) \text{I}\left(\frac{1+q}{2-q}, \frac{2\sqrt{zz_0\xi}}{1-\xi}\right)$$

$$z(p) = 2 p^{2-q} / \left((2-q) \sqrt{D_p^* t_{\text{esc}}} \right)$$

$$\xi(t) = \exp\left(2(q-2) D_p^* t / \sqrt{D_p^* t_{\text{esc}}}\right)$$

where $\text{I}(\nu, x)$ is the modified Bessel function of the first kind, and we recall that D_p^* and t_{esc}^* are defined respectively by relations (15) and (12).

G_2 gives the distribution of particles remaining in the bubble. One can also evaluate the rate of particles escaping the bubble by dividing G_2 by the (momentum-dependent) escape time (11):

$$\dot{G}_{2,\text{esc}}(p, p_0, t) = \frac{G_2(p, p_0, t)}{t_{\text{esc}}(p)} = \frac{p^{2-q} G_2(p, p_0, t)}{t_{\text{esc}}^*}. \quad (19)$$

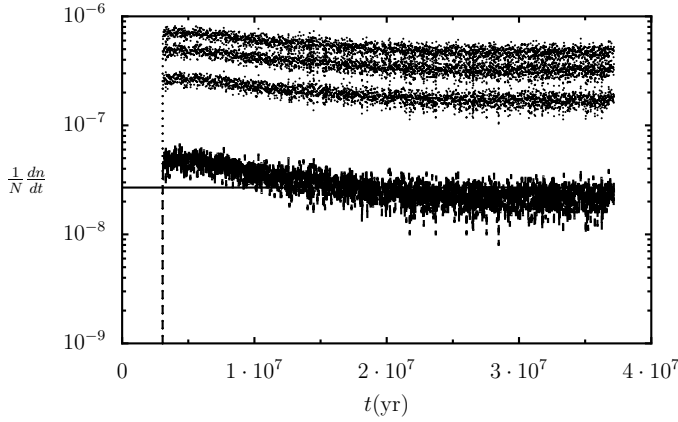


Fig. 3. Mean supernovae rate as a function of time. For each cluster $N_\star = 100$ stars are randomly chosen in the IMF. The central curve represents the experimental mean rate of supernovae after $N_{\text{OB}} = 1000$ samples (with resolution $dt = 10^4$ years). The top curves show 1-, 2-, 3-sigma standard deviations over the clusters set. The solid curve is the theoretical mean rate of supernovae over the cluster's active lifetime (2), ie $N_\star / (t_{\text{SN,max}} - t_{\text{SN,min}})$.

3. Results

3.1. Distribution of supernovae shocks

Before showing the spectra of particles, we discuss briefly the temporal distribution of shocks during the life of the cluster, as it controls the possibility of repeated acceleration.

3.1.1. Rate of supernovae

As an illustration of our Monte-Carlo procedure, if we count the number of supernovae in each time bin $[t, t + dt]$, we get an estimate of the mean supernovae rate. The result is shown on Fig. 3. In agreement with the "instantaneous burst" model of Cerviño et al. (2000), we observe that the distributions of masses and lifetimes combine in such a way that, but for a peak at the beginning, the rate of supernovae is fairly constant during the cluster's life, and can be expressed as a first approximation as

$$\frac{dn_{\text{SN}}}{dt} \simeq \frac{N_\star}{\Delta t_{\text{OB}}^\star} \simeq N_\star \times 3.10^{-8} \text{ yr}^{-1} \quad (20)$$

where we recall that $\Delta t_{\text{OB}}^\star$ is the active lifetime of the cluster, given by Eq. (2).

3.1.2. Typical time between shocks

Knowledge of the time distribution of supernovae is important regarding acceleration in superbubbles, as depending on the typical interval between shocks, accelerated particles may or may not remain within the bubble between two supernovae explosions, and thus experience repeated acceleration². We thus monitor the time interval Δt_{SN} between two *successive* supernovae. The result is shown on Fig. 4. Note that (i) the most probable time interval between two shocks is nothing but the average time between two supernovae $\bar{\Delta t}_{\text{SN}} = \Delta t_{\text{OB}}^\star / N_\star$; and (ii) when time intervals are normalised by this quantity, distributions all have

² Note that this will also strongly depend on the initial energy of the particles: the higher the energy they have gained from one shock, the sooner they will escape the bubble, and hence the less chance they have to be re-accelerated by a subsequent shock.

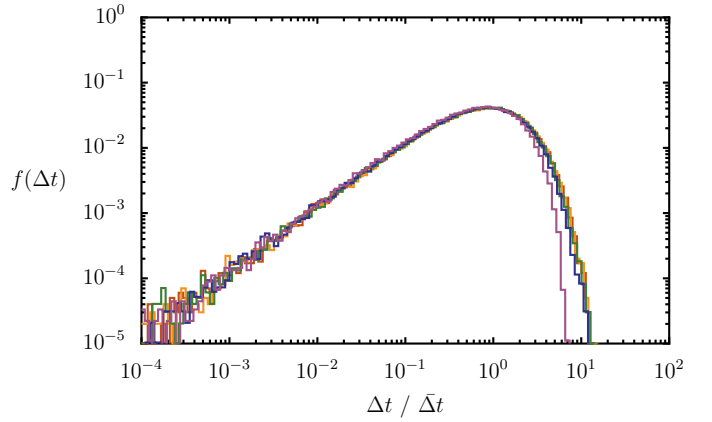


Fig. 4. Distribution of the interval between two successive shocks (normalised to the average interval between two supernovae). For each cluster the interval between two *successive* supernova is monitored, within the numerical resolution $d \log \Delta t = 0.05$. Colour codes different numbers of stars N_\star , logarithmically sampled between 10 and 500 (purple = 10, blue = 27, green = 71, orange = 189, red = 500).

the same shape independently of the number of stars (but for very low numbers of stars).

In order to investigate the probability of acceleration by *many* successive shocks, we have now to compute the maximum time Δt_{max} a particle has to wait *within* a sequence of n *successive* shocks. Only particles whose escape time is more than this value may experience acceleration by n shocks. As previously all distributions have the same shape once time intervals are normalised by $\bar{\Delta t}_{\text{SN}}$, and are very peaked, but now the most probable value of Δt_{max} is a few times bigger than the average value (the more successive shocks we consider, the more chance we have to get an unusually long time interval between any two of them). This is summarised on Fig. 5, which shows the most probable value of Δt_{max} as a function of the number of successive shocks. Note that Δt_{max} may reach 10 times $\bar{\Delta t}_{\text{SN}}$, and that it is all the more an imprecise indicator as N_\star and n are low.

3.2. Average cosmic-ray spectra

3.2.1. General trends

Resulting proton spectra for clusters of two different sizes inside a typical superbubble are shown on Fig. 6. For a given sample, spectra are strongly intermittent during the cluster lifetime (from blue to red), especially at early times. Still, we clearly see convergence to an average spectrum as we increase the number N of samples (from top to bottom). Comparing results for 10 and 100 stars (left and right), we see that what actually matters is the total number of supernovae $N \times N_\star$. The limit spectrum exhibits a distinctive two-parts shape, with a transition from a hard regime (flat spectrum, of slope $s < 4$) to a soft regime (steep spectrum, of slope $s \geq 4$). We also show the escaping spectra on Fig. 7. We see that they have the same overall shape, but are a bit harder (as highly energetic particles escape first) and of much lower normalization.

Hard spectra at low energies are due to combined effects of acceleration by supernova shocks (Fermi 1) and re-acceleration by turbulence (Fermi 2). Soft spectra at high energies are mostly shaped by escape, which removes preferentially highly energetic particles. The transition energy is controlled by a balance be-

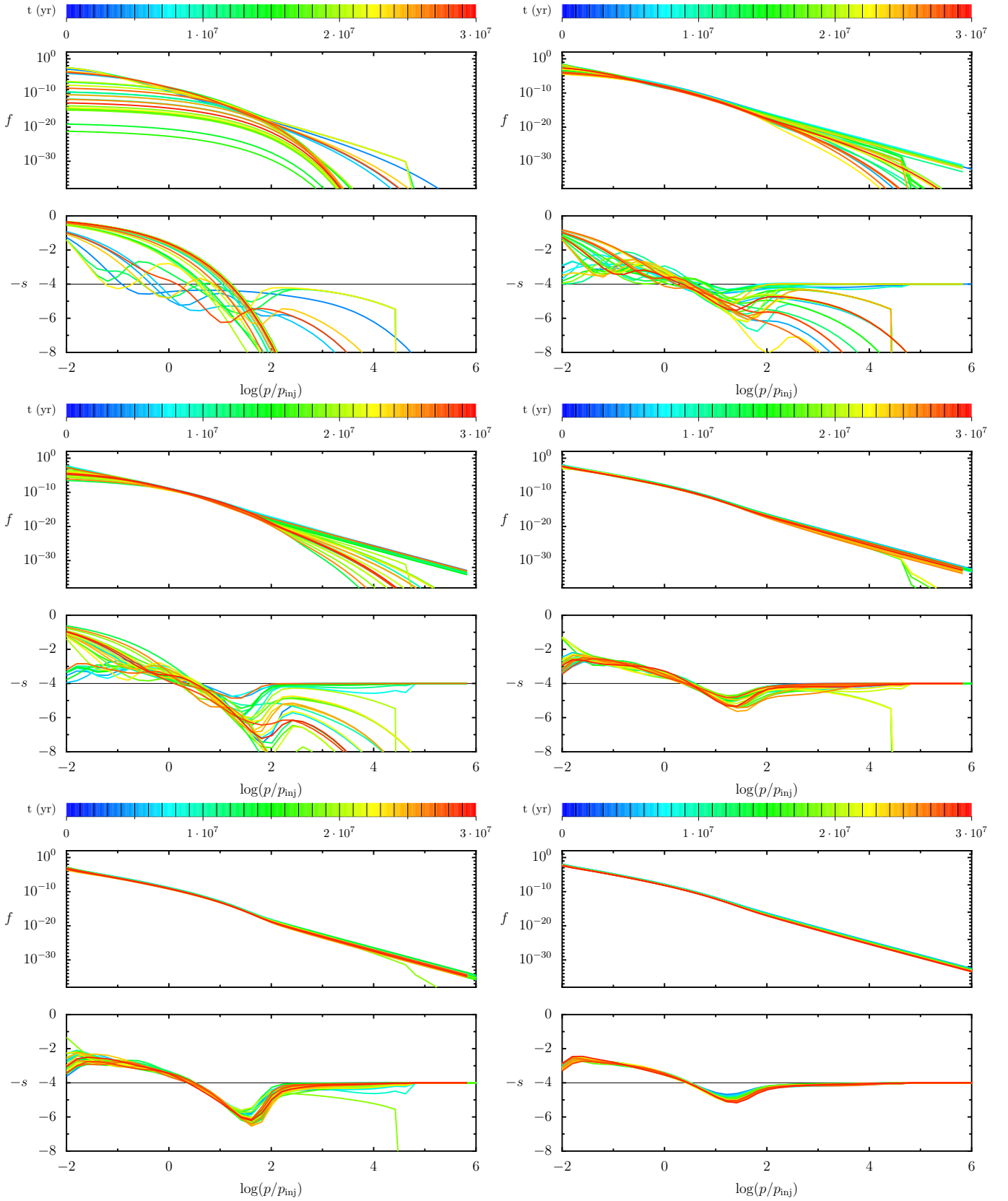


Fig. 6. Sample results of average spectra of cosmic-rays inside the superbubble. The particles spectrum f and its logarithmic slope $s = d \log f / d \log p$ are plotted versus momentum p . The size of the cluster is $N_\star = 10$ (left) and $N_\star = 100$ (right). The number of samplings rises from top to bottom: $N = 10, 100, 1000$. Other parameters are $q = 5/3$, $B = 10 \mu\text{G}$, $\eta_T = 1$, $\lambda_{\text{max}} = 10 \text{ pc}$, $x_{\text{acc}} = 40 \text{ pc}$, $n = 10^{-2} \text{ cm}^{-3}$.

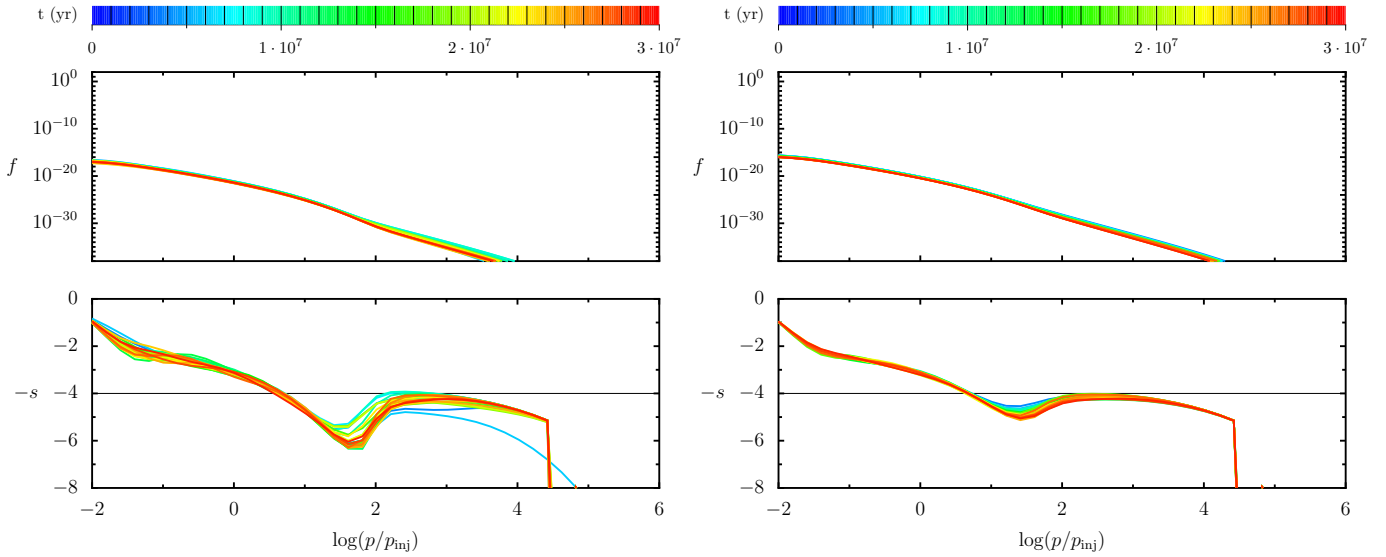


Fig. 7. Sample results of average spectra of cosmic-rays escaping the superbubble. The particles spectrum f per unit time and its logarithmic slope $s = d \log f / d \log p$ are plotted versus momentum p . The size of the cluster is $N_\star = 10$ (left) and $N_\star = 100$ (right). The number of samplings is $N = 1000$. Other parameters are as in figure 6: $q = 5/3$, $B = 10 \mu\text{G}$, $\eta_T = 1$, $\lambda_{\max} = 10 \text{ pc}$, $x_{\text{acc}} = 40 \text{ pc}$, $n = 10^{-2} \text{ cm}^{-3}$.

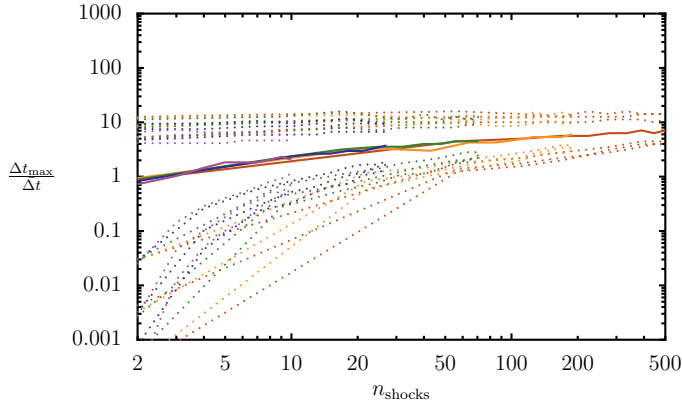


Fig. 5. Maximum time interval between two successive shocks in a sequence of n successive shocks (normalised to the average interval between two supernovae). Solid curves correspond to the most frequent value of Δt_{\max} (ie, maxima of the curves in Fig. 4). Dotted lines give the envelope of the distribution (they correspond to a decrease from the maximum value by a factor of 10, 100, 1000). Colours code the number of stars N_\star in the same way as in Fig. 4 (note that N_\star coincides with the maximum number of successive shocks n for which data are available).

tween re-acceleration and escape timescales, and thus depends on the superbubble parameters.

3.2.2. Parametric study

For each cluster we have to define eight parameters: N_\star , r , q , η_T , B , λ_{\max} , n , x_{acc} , which are more or less constrained. We sample the size of the cluster roughly logarithmically between 10 stars and 500 stars, ie $N_\star = 10, 30, 70, 200, 500$. We consider only strong supernova shocks of $r = 4$. We compare classical turbulence indices $q = 5/3$ (Kolmogorov cascade, K41) and $q = 3/2$ (Kraichnan cascade, IK65). We consider two dif-

ferent scenarii for the magnetic field: if a turbulent dynamo is at work then $B \simeq 10 \mu\text{G}$ and $\delta B \gg B$ so that $\eta_T \simeq 1$ (Bykov 2001), if not then because of the bubble expansion $B \simeq 1 \mu\text{G}$ and $\delta B < B$ (if $\delta B = B/2$ then $\eta_T = 0.2$). The external scale of the turbulence λ_{\max} is at least of the order of the distance d_\star between two stars in the cluster, which, for a typical OB association radius of 35 pc (eg Garmany 1994), and assuming uniform distribution (a quite crude approximation), reads

$$d_\star \simeq \frac{56 \text{ pc}}{N_\star^{1/3}} \quad (21)$$

that is 26, 12, 7 pc for respectively 10, 100, 500 stars. But λ_{\max} will be higher if turbulence is driven by supernova remnants, the radius of which goes roughly as

$$r_{\text{SNR}} \simeq 38 \text{ pc} \left(\frac{t}{10^4 \text{ yr}} \right)^{2/5} \quad (22)$$

in the Sedov-Taylor phase inside a superbubble (Parizot et al. 2004). Hence we vary $\lambda_{\max} = 10, 20, 40, 80 \text{ pc}$. We take the size of the acceleration region to be of the order of the radius of a supernova remnant after our time-step $dt = 10\,000 \text{ yr}$, that is $x_{\text{acc}} = 40 \text{ pc}$ according to Eq. (22). However in evolved superbubbles it might be higher, up to more than 100 pc, so we also try 80 pc and 120 pc. The density inside a superbubble is always low, to assess its influence we run simulations with $n = 10^{-3} \text{ cm}^{-3}$, $n = 5 \cdot 10^{-3} \text{ cm}^{-3}$ and $n = 10^{-2} \text{ cm}^{-3}$. This makes 720 different cases to run. And for each case, we have to set the number N of samplings per cluster: convergence of average spectra typically requires $N_\star \times N \simeq 10^4$, but the general trend is already clear as soon as $N_\star \times N \simeq 10^3$, so we simply take $N = 10^3 / N_\star$.

We thus had to run a lot of simulations to explore the parameters space. But interestingly enough, it turned out that the effects of the 6 parameters relevant to stochastic acceleration and escape: q , η_T , B , λ_{\max} , n , x_{acc} can be summarized through a

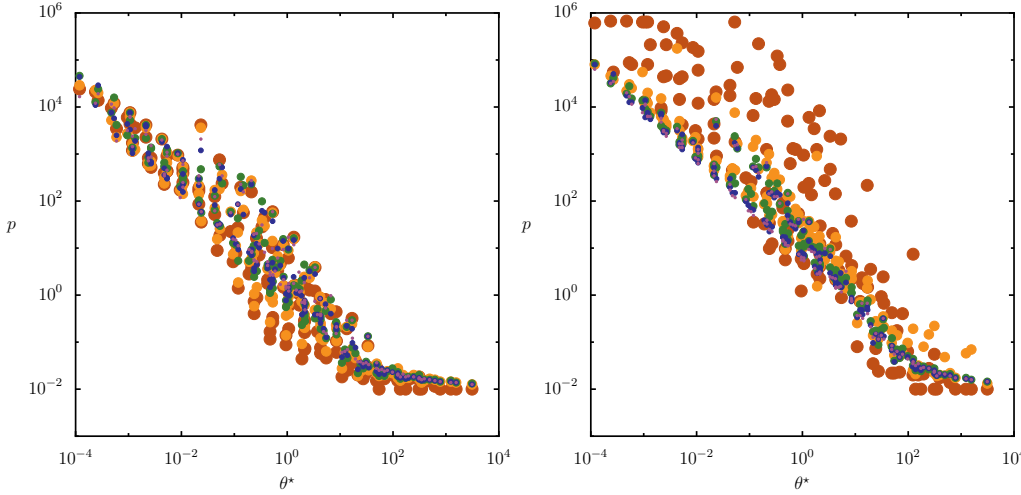


Fig. 8. Hard-soft transition momentum as a function of θ^* and N_* . The transition momentum is defined as the momentum up to which the particles spectrum may have index lower than a given threshold: $s = 3$ at the left, $s = 4$ at the right. θ^* is a dimensionless parameter defined by Eq. (23). The number of stars $N_* = 10, 30, 70, 200, 500$ is coded by both dots sizes and dots colours. Momentum resolution is of 10 bins per decompression shift, that is ≈ 50 bins per decade.

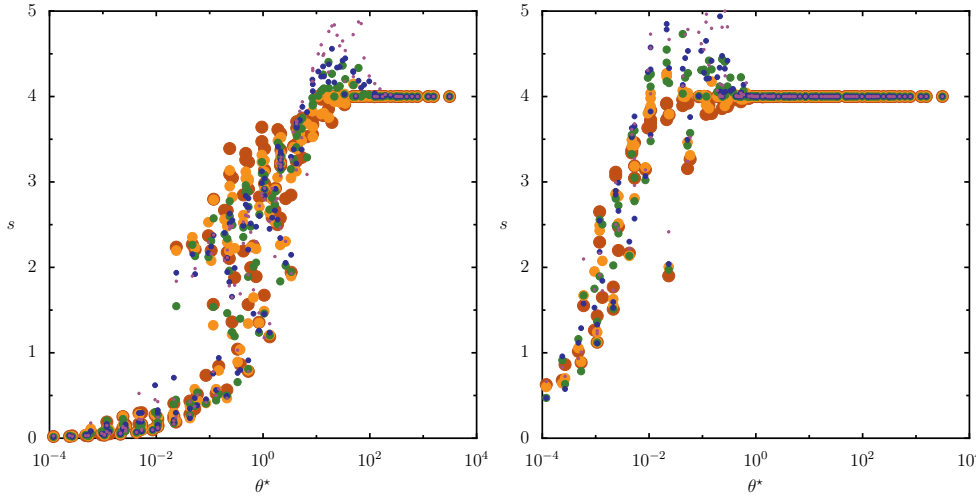


Fig. 9. Lowest slope as a function of θ^* and N_* . The plots show the lowest slope (corresponding to the hardest spectrum) reached at a given momentum: $p = 1$ GeV at the left, $p = 1$ TeV at the right. θ^* is a dimensionless parameter defined by Eq. (23). The number of stars $N_* = 10, 30, 70, 200, 500$ is coded by both dots sizes and dots colours. Momentum resolution is of 10 bins per decompression shift, that is ≈ 50 bins per decade.

single parameter, the adimensional number θ^* introduced by Becker et al. (2006):

$$\theta^* = \frac{1}{D_p^* t_{\text{esc}}^*} \quad (23)$$

which, according to Eq. (15) and (12) goes as

$$\theta^* \propto \eta_T^{-2} B^{2q-6} \lambda_{\text{max}}^{2q-2} x_{\text{acc}}^{-2} n. \quad (24)$$

For standard turbulence indices, we have

$$\theta^* \simeq \begin{cases} \frac{2}{\eta_T^2} \left(\frac{B}{10 \mu\text{G}} \right)^{-\frac{8}{3}} \left(\frac{\lambda_{\text{max}}}{10 \text{ pc}} \right)^{\frac{4}{3}} \left(\frac{x_{\text{acc}}}{40 \text{ pc}} \right)^{-2} \left(\frac{n}{10^{-2} \text{ cm}^{-3}} \right) & q = 5/3 \\ \frac{10^{-2}}{\eta_T^2} \left(\frac{B}{10 \mu\text{G}} \right)^{-3} \left(\frac{\lambda_{\text{max}}}{10 \text{ pc}} \right) \left(\frac{x_{\text{acc}}}{40 \text{ pc}} \right)^{-2} \left(\frac{n}{10^{-2} \text{ cm}^{-3}} \right) & q = 3/2 \end{cases} \quad (25)$$

With all the possible superbubble parameters considered here, θ^* ranges from 10^{-4} to 10^{+4} . As we consider only strong supernova shocks of $r = 4$, the single remaining parameter is the number of stars N_* (represented through dots of different colours and sizes on the subsequent plots), which has a weaker impact on results.

To characterize the spectra of accelerated particles, we use two indicators, plotted on Figs. 8 and 9. We have checked that the results are independent of the resolution provided that there is at least a few bins per decompression shift. The residual variability seen mostly derives from the simulation procedure itself,

which is based on random samplings. On Fig. 8 we show the momentum of transition from hard to soft regimes, defined as the maximum momentum up to which the slope may be smaller than a given value (3 or 4 here). Above this momentum, the slope always remains greater than this value. Below this momentum, the slope can be as low as 0, meaning that particles pile-up from injection – but note that it can also happen to be ≥ 4 at a particular time in a particular cluster sample, as distributions are intermittent. As θ^* increases the transition momentum falls exponentially from almost the maximum momentum considered (a fraction of PeV) down to the injection momentum (10 MeV). For rule-of-thumb calculations one can say that the slope can get < 3 up to $p = 1/\theta^*$ GeV. On Fig. 9 we show the lowest slope (corresponding to the hardest spectrum) obtained at a fixed momentum (1 GeV and 1 TeV here). As θ^* increases the lowest slope rises from 0 (which is possible in the case of stochastic re-acceleration) to 4 (the canonical value for single regular acceleration in the test particle case). As expected the critical θ^* between hard and soft regimes decreases as we increase the reference momentum: the break occurs around $\theta^* = 10$ for $p = 1$ GeV and around $\theta^* = 0.01$ for $p = 1$ TeV.

This overall behaviour can be explained, noting that θ^* is roughly the ratio of the re-acceleration time and of the escape time. Low θ^* are obtained when re-acceleration is faster than

escape, allowing Fermi processes to build hard spectra up to high energies, as particles get re-accelerated by shocks and/or turbulence; high θ^* are obtained when escape is faster than re-acceleration, resulting in always quite soft in-situ spectra, as particles escape immediately after being accelerated by a supernova shock. $\theta^* = 1$ corresponds to a balance between gains and losses, in that particular case the spectral break occurs around 10 GeV for $s > 4$ and 1 GeV for $s > 3$.

4. Application

4.1. A selection of massive star regions

In this section we have gathered the physical parameters of some well observed massive star clusters and their associated superbubbles. The reliability and the completeness of the data were our main selection criteria. The parameters useful for our study are: the cluster composition (number of massive stars), age, distance, size, and the superbubble size and density. Note that we are biased towards young objects, as older ones are more difficult to isolate because of large extensions and sequential formations. Information on density is sometimes lacking. The density can span several orders of magnitude, usually between 10^{-2} and 10 cm^{-3} in the central cluster (Torres et al. 2004) and between 10^{-3} and 10^{-1} cm^{-3} in the superbubble (Parizot et al. 2004). If X-ray observations are available, it can be indirectly estimated from the thermal X-ray spectrum, given the plasma temperature and the column density along the line of sight. In the case of complete lack of data, we accept a mean density between $5.10^{-3} \text{ cm}^{-3}$ and $5.10^{-2} \text{ cm}^{-3}$. Unfortunately, the magnetic field parameters are not directly measured, so that we consider different limiting scenarios: $B = 1 \mu\text{G}$ and $\eta_T = 0.2$ if the turbulence is low, $B = 10 \mu\text{G}$ and $\eta_T = 1$ if the turbulence is high. In each case we compare turbulence indices $q = 5/3$ and $q = 3/2$. The maximal scale of the turbulence λ_{max} may be taken to be as small as the size of the stellar cluster (especially in the case where few supernovae have already occurred), or as big as the size of the superbubble itself.

These quantities are used to estimate the key parameter θ_* in each of the selected objects using Eq. (25). All the parameters and results are summarised in table 1. Before discussing the implications of these values, we give more details on the selected regions in the following two sections, regarding clusters found respectively in our Galaxy and in the Large Magellanic Cloud (LMC).

4.1.1. Galaxy

- Cygnus region: in this region we distinguish two distinct objects, the clusters Cygnus OB1 and OB3, which have blown a common superbubble, and the cluster Cygnus OB2. Note that the latter has been detected at TeV energies by Hegra (Aharonian et al. 2005), which reported on an extended source (TeV J2032+4130), and by Milagro (Abdo et al. 2007), which reported on extended diffuse emission and at least one TeV source (MGRO J2019+37). A supershell has also been detected around the Cygnus X-ray superbubble, it may have been blown by a sequence of starbursts, Cygnus OB2 being the very last.
- Orion OB1: this association is composed of several sub-groups (Brown et al. 1999), the age selected here of 12 Myrs corresponds to the oldest one (OB1a).

- Carina nebula: this region is one of the most massive star forming regions in our Galaxy. It contains two massive stellar clusters: Trumpler 14 and Trumpler 16 (Smith et al. 2000), of cumulative size of approximately 10 pc.
- Westerlund 1: this cluster is very compact although it harbours hundreds of massive stars. The size of the superbubble is uncertain, we accept here the value of 40 pc reported by Kothes & Dougherty (2007) for the HI shell surrounding the cluster. Note that Westerlund 1 has been detected recently by HESS (Ohm et al. 2009).
- Westerlund 2: the distance to this cluster is still a matter of debate (see the discussion in Aharonian et al. 2007), we adopt here the estimate of Rauw et al. (2007), and use it to reevaluate the size obtained by Conti & Crowther (2004). We accept the giant HII region RCW49 of size 100 pc as the structure blown by Westerlund 2. Tsujimoto et al. (2007) have provided spectral fit of the diffuse X-ray emission from RCW49, from which we deduce a density $\sim 1, 5.10^{-3} \text{ cm}^{-3}$. Note that Westerlund 2 has been detected recently by HESS (Aharonian et al. 2007).

4.1.2. Large Magellanic Cloud

All density estimates here have been derived from observations of diffuse X-ray emission (at the distance to the LMC these observations usually cover the entire structure, so that the density deduced is an average over the OB association and the ionised region around it).

- DEML 192: this region harbours two massive star clusters, LH 51 and 54 (Lucke & Hodge 1970). The spatial extension of both clusters has been deduced from Oey & Smedley (1998) but is likely an over-estimate as the frontier of the clusters are not well defined.
- 30 Doradus: this region is quite complex as can be seen from recent Chandra observations (Townsend et al. 2006). In particular the superbubble extension is difficult to estimate precisely. We decided to keep the value given for the 30 Doradus nebula by Walborn (1991). Also the extension of the star cluster may be larger than the core which harbours several thousand of stars (Massey & Hunter 1998). The core size is $\leq 10 \text{ pc}$ (Massey & Hunter 1998), even estimated to be $\sim 2 \text{ pc}$ by Walborn (1991). The number of massive stars in R136 depends on the cluster total mass, estimated between $5.10^4 M_\odot$ and $2, 5.10^5 M_\odot$. Using a Salpeter IMF, one finds $N_*(M > 8M_\odot) \simeq 400 - 2700$. Notice that the stellar formation in 30 Doradus is sequential and has started more than 10 Myrs ago (Massey & Hunter 1998).
- N11: this giant HII region harbours several star clusters LH9, LH10, LH13 and LH14, probably produced as a sequence of starbursts (Walborn et al. 1999). Here we mostly consider the star cluster LH9 at the center of N11 and the shell encompassing it (shell 1 in Mac Low et al. 1998). LH10 is a younger star cluster with an estimated age of 1 Myr (Walborn et al. 1999), in which no supernova has yet occurred. The other clusters are less powerful.

4.2. Discussion

In table 1 we see that in all cases except for $q = 3/2$, $B = 10 \mu\text{G}$ the critical momentum $\sim 1/\theta_*$ GeV is in the non-relativistic regime. Then even if at lower energies the particle distribution is hard, as pressure is always dominated by relativistic particles, one should not expect strong back-reaction of accelerated parti-

Name	Cluster				Superbubble		θ_*			
	N_*	Age (Myr)	Distance (kpc)	Size (pc)	Size (pc)	Density (cm ⁻³)	B=1μG q = 5/3	B=1μG q = 3/2	B=10μG q = 5/3	B=10μG q = 3/2
Cygnus OB1/3	38 ⁽¹⁶⁾	2-6 ⁽¹²⁾	1.8 ⁽¹⁹⁾	24	80-100 ⁽¹⁴⁾	0.01?	5.10 ⁴ 5.10 ⁵	4.10 ² 3.10 ³	4.10 ⁰ 4.10 ¹	2.10 ⁻² 1.10 ⁻¹
Cygnus OB2	750 ⁽⁵⁾	3-4 ⁽¹²⁾	1.4-1.7 ⁽¹⁰⁾	60 ⁽¹¹⁾	450? ⁽⁵⁾	0.02 ⁽⁵⁾	2.10 ⁴ 2.10 ⁵	9.10 ¹ 7.10 ²	1.10 ⁰ 2.10 ¹	4.10 ⁻³ 3.10 ⁻²
Orion OB1	30-100 ⁽³⁾	12 ⁽²⁾	0.45 ⁽²⁾	10 ⁽²⁾	140x300 ⁽³⁾	0.02-0.03 ⁽⁴⁾	3.10 ³ 2.10 ⁶	4.10 ¹ 7.10 ³	3.10 ⁻¹ 2.10 ²	1.10 ⁻³ 3.10 ⁻¹
Carina nebula	?	3 ⁽²³⁾	2.3 ⁽⁸⁾	20	110 ⁽²³⁾	0.01?	2.10 ⁴ 2.10 ⁶	1.10 ² 7.10 ³	1.10 ⁰ 1.10 ²	5.10 ⁻³ 3.10 ⁻¹
Westerlund 1	450 ⁽¹⁾	3.3 ⁽¹⁾	3.9 ⁽¹³⁾	1 ⁽¹⁾	40? ⁽¹³⁾	0.01?	2.10 ³ 3.10 ⁶	5.10 ¹ 2.10 ⁴	2.10 ⁻¹ 3.10 ²	2.10 ⁻³ 8.10 ⁻¹
Westerlund 2	14 ⁽²¹⁾	2 ⁽²¹⁾	8 ⁽²¹⁾	1 ⁽⁶⁾	100 ^(21,6)	0.0015 ⁽²⁴⁾	1.10 ² 5.10 ⁴	2.10 ⁰ 2.10 ²	9.10 ⁻³ 4.10 ⁰	1.10 ⁻⁴ 1.10 ⁻²
DEM L192	135	3 ⁽²⁰⁾	50	60 ⁽²⁰⁾	120x135 ⁽⁹⁾	0.03 ⁽⁷⁾	3.10 ⁵ 1.10 ⁶	2.10 ³ 4.10 ³	2.10 ¹ 9.10 ¹	6.10 ⁻² 2.10 ⁻¹
30 Doradus	> 400 ⁽²²⁾	2 ⁽¹⁷⁾	50	40 ⁽²⁵⁾	200 ⁽²⁵⁾	0.09 ⁽²⁷⁾	2.10 ⁵ 2.10 ⁶	1.10 ³ 7.10 ³	2.10 ¹ 2.10 ²	6.10 ⁻² 3.10 ⁻¹
N11	130	5 ⁽²⁶⁾	50	15x30 ⁽¹⁸⁾	100x150 ⁽⁹⁾	0.08 ⁽¹⁵⁾	9.10 ⁴ 4.10 ⁶	9.10 ² 2.10 ⁴	8.10 ⁰ 4.10 ²	3.10 ⁻² 8.10 ⁻¹

Table 1. Relevant physical parameters for well observed massive star forming regions in the Galaxy and in the LMC, and the corresponding estimates of θ_* from Eq. (25), as explained in section 4.1 (the range of values of θ_* given for each object for each magnetic configuration reflects uncertainties in the actual values of bubble density, accelerator size and turbulence scale). N_* is the number of massive stars with masses $\geq 8M_\odot$ (a Salpeter IMF has been assumed expected for N11 where an index of 2.4 has been used). Sizes are either the diameter if the region is spherical or the big and small semi-axis if the region is ellipsoidal. The density is the Hydrogen nuclei density. References: (1) Brandner et al. (2008), (2) Brown et al. (1994), (3) Brown et al. (1995), (4) Burrows et al. (1993), (5) Cash et al. (1980), (6) Conti & Crowther (2004), (7) Cooper et al. (2004), (8) Davidson & Humphreys (1997), (9) Dunne et al. (2001), (10) Hanson (2003), (11) Knödlseider (2000), (12) Knödlseider et al. (2002), (13) Kothes & Dougherty (2007), (14) Lozinskaya et al. (1998), (15) Maddox et al. (2009), (16) Massey et al. (1995), (17) Massey & Hunter (1998), (18) Nazé et al. (2004), (19) Nichols-Bohlin & Fesen (1993), (20) Oey & Smedley (1998), (21) Rauw et al. (2007), (22) Selman et al. (1999), (23) Smith et al. (2000), (24) Tsujimoto et al. (2007), (25) Walborn (1991), (26) Walborn & Parker (1992), (27) Wang & Helfand (1991).

cles over the fluid inside the superbubble, compared to the case where collective acceleration effects are not taken into account. However if the magnetic field pressure is close to equipartition with the thermal pressure as suggested by Parizot et al. (2004), and provided that the turbulence index q is low enough, then the impact of particles on their environnement has to be investigated. More generally, if q is low enough and/or B is high enough, then the superbubble can no longer be regarded as a sum of isolated supernovae, but acts a global accelerator, producing hard spectra over a wide range of momenta.

One can wonder how solid these results are, given all the uncertainties in the data. In particular, the parameter θ_* is very sensitive to the accelerator size x_{\max} . However x_{\max} can not be much lower than a few tens of parsecs (the typical size of the OB association) and can not be much larger than 100 pc (the typical size of the superbubble). The maximal scale of the turbulence, λ_{\max} , is even more difficult to estimate, but it also ranges between those extrema. Determining precisely these spatial scales is complicated by the difficulty to estimate the supershell associated with a given cluster, all the more so since multiple bursts episodes have occurred (as is likely the case in 30 Doradus). θ_* is also directly proportional to the density, which is not always measured with good accuracy, but which can usually be rather well constrained within one order of magnitude. The upper and lower values of θ_* given in table 1 reflect the uncertainties of these three key parameters. In the end, we believe that the results presented in table 1 provide a good hint of whether collective effects will dominate inside the superbubble or not. In

the range of physical parameters allowed for sizes and densities, the main uncertainty on the critical parameter θ_* is clearly due to our poor knowledge of the magnetic field (how high is the field, how turbulent it is). It can be seen from table 1 that for a given prescription of the magnetic turbulence, the values obtained for both Galactic and LMC clusters are not very different from one another.

5. Limitations and possible extensions

5.1. Regarding shock acceleration physics

The potentially biggest limitation in our model is the use of a linear model for regular acceleration: we have not considered the back-reaction of accelerated particles on their accelerator, whereas cosmic-rays may easily modify the supernova remnant shock and therefore the way they are themselves accelerated (Malkov & Drury 2001). As non-linear acceleration is a difficult problem, only a few models are available, like the time-asymptotic semi-analytical models of Berezhko & Ellison (1999) or Blasi & Vietri (2005), and the time-dependent numerical simulations of Kang & Jones (2007) or Ferrand et al. (2008). We will include one of these non-linear approaches in our Monte-Carlo framework to extend our current work. We can already note that non-linear effects tend to produce concave spectra, softer at low energies and harder at high energies than

the canonical power-law spectrum, and thus may compete with re-acceleration and escape effects, which we have shown to have opposite effects. Moreover non-linearity is also at play regarding the turbulent magnetic field (mandatory for Fermi process to scatter off particles), which remarkably can be produced by energetic particles themselves through various instabilities. This difficult and still quite poorly understood process has recently lead to a great deal of efforts, through the use of MHD simulations (Jones & Kang 2006), semi-analytical models (Amato & Blasi 2006) or Monte-Carlo simulations (Vladimirov et al. 2006).

Another limitation is that only strong primary supernova shocks have been considered here (of compression ratio $r = 4$), but as superbubbles are very clumpy and turbulent media many weak secondary shocks are also expected (of $r < 4$). The compression ratio r depends on the Mach number M_S as

$$r = \frac{4 M_S^2}{M_S^2 + 3} \quad (26)$$

with

$$M_S = \frac{v_S}{c_S} \simeq 50 \left(\frac{v_S}{5000 \text{ km/s}} \right) \left(\frac{T}{10^6 \text{ K}} \right)^{-1/2} \quad (27)$$

where u_S is the shock velocity (of many thousands of km/s in the early stages of a remnant evolution) and c_S is the speed of sound in the unperturbed upstream medium (as high as a few hundreds of km/s in a superbubble because of the high temperature T of a few millions of Kelvin). In the linear regime the slope of accelerated particles is determined solely by r according to Eq. (5). In superbubbles primary supernova shocks have $M_S \simeq 50$ and already $r \simeq 4$, leading to $s \simeq 4$; but a secondary shock of say $M_S \simeq 5$ has only $r \simeq 3$, leading to $s \simeq 4.5$. We note that although weaker shocks produce softer individual spectra, being more numerous they may help producing hard spectra through repeated acceleration, so that their net effect is not obvious. To begin their investigation we have added a weak shock in each time-step immediately following a supernova (but if another supernova occurs at that moment), of compression ratio randomly chosen between 1.5 and 3.5. Regarding regular acceleration alone, important differences are seen between simulations including only strong shocks, or only weak shocks, or both. But once combined with stochastic acceleration and escape, these differences seem to be smoothed out. We have run our 720 simulations at medium resolution again, and we have observed that our two indicators (momentum of transition and minimal slope) remain globally unchanged. The shape of cosmic-ray spectra thus seems to be mostly determined by the interplay between re-acceleration and escape, acceleration at shock fronts acting mostly as an injector of energetic particles. Note that, before supernova explosions, the winds of massive stars, not explicitly considered in this study, may also act as injectors in the same way, as they have roughly the same mechanical power integrated over the star lifetime.

Finally we may put into question our particular choice of stellar evolution models, but we believe that possible variations in the exact lifetime of massive stars would bring only higher order corrections to the general picture we have obtained. We also note that we have implicitly considered that stars are born at the same time, and then evolve independently, while in reality star formation may occur through successive bursts within a same molecular cloud, which could be sequentially triggered by the first explosions of supernovae. Another possible amendment to our model is the fact that stars of mass greater than 40 solar masses may end their life without collapsing, and thus without

launching a shock. We have run our 720 simulations at low resolution again, considering the occurrence of supernovae only for $m < 40 m_\odot$, and have checked that our two indicators remain globally unchanged. This seems consistent with the shape of the IMF (there are very few stars of very high mass) and the shape of star lifetimes (stars of very high mass have roughly the same lifetime).

5.2. Regarding inter-shocks physics

We use an approximate model for stochastic acceleration, because of the use of relativistic formulae and the neglect of energy losses, in order to fit with Becker et al. (2006) analytical results. But note that regarding stochastic acceleration the relativistic regime actually requires $m_p v \gg m_p v_A$ where v is the particle velocity and v_A the Alfvén velocity

$$v_A = \frac{B}{\sqrt{\mu_0 \rho}} \simeq 2.10^7 \text{ cm.s}^{-1} \left(\frac{B}{10 \mu\text{G}} \right) \left(\frac{n}{10^{-2} \text{ cm}^{-3}} \right)^{-\frac{1}{2}}, \quad (28)$$

which holds as soon as $p \gg 1$ MeV in a superbubble as $v_A/c \simeq 10^{-3}$. Although we could of course implement more involved models of transport, we would like to stress that our main objective was to find the key dependences of the problem, and we have shown that it is mainly controlled by the parameter θ^* . Regarding losses, the formalism of Becker et al. (2006) allows for systematic losses, but for mathematical convenience these are supposed to occur at a rate $\propto p^{q-1}$, which can describe Coulomb losses only in the very special case $q = 2$. But proton losses above 1 GeV are dominated by nuclear interactions (Aharonian & Atoyan 1996), with a typical lifetime of $6.10^7 \text{ yr}/n$ where n is the density in cm^{-3} , which is far longer than the superbubble lifetime given the low density $n \leq 10^{-2} \text{ cm}^{-3}$ (however this might be a concern when cosmic-rays reach the parent molecular clouds where $n > 10^2 \text{ cm}^{-3}$). At the very low end of CR spectra (around the MeV), ionization losses might also come to play and compete with stochastic re-acceleration.

Finally we note that most parameters are actually time-dependent, and might in fact become considerably different in late stages (for completeness we have run our simulations until the explosion of the longest lived stars, but over tens of millions of years the overall morphology and properties of the superbubble might change substantially as it interacts with its environment). As long as the typical evolution timescale of relevant parameters is bigger than our time-step $dt = 10\,000 \text{ yr}$, their variation can be taken into account simply by varying the value of θ^* accordingly. Otherwise, direct time-dependent numerical simulations of the kind of Ferrand et al. (2008) will be necessary.

6. Conclusions

Our main conclusions are as follows:

1. cosmic-ray spectra inside superbubbles are strongly intermittent (at a given time they depend on the particular history of a given cluster);
2. still, spectra follow a distinctive overall trend, resulting from a competition between (re-)acceleration by regular and stochastic Fermi processes and escape: they are harder at lower energies ($s < 4$) and softer at higher energies ($s > 4$) – a shape in agreement with the results of Bykov (2001), obtained under different assumptions³;

³ Bykov (2001) considers acceleration of particles by large-scale motions of the magnetized plasma inside the superbubble, which de-

3. the momentum at which this spectral break occurs critically depends on the bubble parameters: it increases when the magnetic field value and acceleration region size increase, and decreases when the density and the turbulence external scale increase – all these effects being summarized by the single dimensionless parameter θ^* defined by Eq. (23);
4. for reasonable values of superbubble parameters, very hard spectra ($s < 3$) can be obtained over a large range of energies, provided superbubbles are highly magnetized and turbulent (which is a debated issue).

These results have important implications on the chemistry inside superbubbles and on the high-energy emission from these objects. For instance, in the superbubble Perseus OB2 there is observational evidence for intense spallation activity Knauth et al. (2000), attributed to a high density of low-energy cosmic-rays, but EGRET has not detected π^0 -decay radiation, which puts strong limits on the density of high-energy cosmic-rays. This is consistent with the shape of the spectra obtained in this work. We are thus looking forward to see how new instruments such as AGILE and Fermi, and in mid-term perspective the Cerenkov Telescope Array (C.T.A.), will perform on such extended sources as massive star forming regions, which have recently emerged as very high-energy sources. With that respect, we make a final comment that the high intermittency of predicted spectra might explain the puzzling fact that some objects are detected while others remain unseen.

Acknowledgements. The authors would like to thank Isabelle Grenier and Thierry Montmerle for sharing their thoughts on the issues investigated here.

References

- Abdo, A. A., Allen, B., Berley, D., et al. 2007, *ApJ*, 658, L33
- Achterberg, A. 1990, *A&A*, 231, 251
- Aharonian, F., Akhperjanian, A., Beilicke, M., et al. 2005, *A&A*, 431, 197
- Aharonian, F., Akhperjanian, A. G., Bazer-Bachi, A. R., et al. 2007, *A&A*, 467, 1075
- Aharonian, F. A. & Atoyan, A. M. 1996, *A&A*, 309, 917
- Amato, E. & Blasi, P. 2006, *MNRAS*, 371, 1251
- Becker, P. A., Le, T., & Dermer, C. D. 2006, *ApJ*, 647, 539
- Berezhko, E. G. & Ellison, D. C. 1999, *ApJ*, 526, 385
- Blasi, P. & Vietri, M. 2005, *ApJ*, 626, 877
- Brandner, W., Clark, J. S., Stolte, A., et al. 2008, *A&A*, 478, 137
- Brown, A. G. A., Blaauw, A., Hoogerwerf, R., de Bruijne, J. H. J., & de Zeeuw, P. T. 1999, in *NATO ASIC Proc. 540: The Origin of Stars and Planetary Systems*, ed. C. J. L. N. D. Kylafis, 411
- Brown, A. G. A., de Geus, E. J., & de Zeeuw, P. T. 1994, *A&A*, 289, 101
- Brown, A. G. A., Hartmann, D., & Burton, W. B. 1995, *A&A*, 300, 903
- Burrows, D. N., Singh, K. P., Nousek, J. A., Garmire, G. P., & Good, J. 1993, *ApJ*, 406, 97
- Butt, Y. 2009, *Nature*, 460, 701
- Bykov, A. M. 2001, *Space Science Reviews*, 99, 317
- Cash, W., Charles, P., Bowyer, S., et al. 1980, *ApJ*, 238, L71
- Casse, F., Lemoine, M., & Pelletier, G. 2002, *Phys. Rev. D*, 65, 023002 1
- Cerviño, M., Knödseder, J., Schaerer, D., von Ballmoos, P., & Meynet, G. 2000, *A&A*, 363, 970
- Conti, P. S. & Crowther, P. A. 2004, *MNRAS*, 355, 899
- Cooper, R. L., Guerrero, M. A., Chu, Y.-H., Chen, C.-H. R., & Dunne, B. C. 2004, *ApJ*, 605, 751
- Davidson, K. & Humphreys, R. M. 1997, *ARA&A*, 35, 1
- Drury, L. O. 1983, *Reports on Progress in Physics*, 46, 973
- Dunne, B. C., Points, S. D., & Chu, Y.-H. 2001, *ApJS*, 136, 119
- Ferrand, G., Downes, T., & Marcowith, A. 2008, *MNRAS*, 383, 41
- Garmany, C. D. 1994, *PASP*, 106, 25
- Hanson, M. M. 2003, *ApJ*, 597, 957
- Higdon, J. C. & Lingenfelter, R. E. 2005, *ApJ*, 628, 738
- Jones, T. W. & Kang, H. 2006, *Cosmic Particle Acceleration*, 26th meeting of the IAU, Joint Discussion 1, 16-17 August, 2006, Prague, Czech Republic, JD01, #41, 1
- Kang, H. & Jones, T. W. 2007, *Astroparticle Physics*, 28, 232
- Klepach, E. G., Ptuskin, V. S., & Zirakashvili, V. N. 2000, *Astroparticle Physics*, 13, 161
- Knauth, D. C., Federman, S. R., Lambert, D. L., & Crane, P. 2000, *Nature*, 405, 656
- Knödseder, J. 2000, *A&A*, 360, 539
- Knödseder, J., Cerviño, M., Le Duigou, J.-M., et al. 2002, *A&A*, 390, 945
- Kothes, R. & Dougherty, S. M. 2007, *A&A*, 468, 993
- Kroupa, P. 2002, *Science*, 295, 82
- Limongi, M. & Chieffi, A. 2006, *ApJ*, 647, 483
- Lozinskaya, T. A., Pravdikova, V. V., Sitnik, T. G., Esipov, V. F., & Mel'Nikov, V. V. 1998, *Astronomy Reports*, 42, 453
- Lucke, P. B. & Hodge, P. W. 1970, *AJ*, 75, 171
- Mac Low, M.-M., Chang, T. H., Chu, Y.-H., et al. 1998, *ApJ*, 493, 260
- Maddox, L. A., Williams, R. M., Dunne, B. C., & Chu, Y.-H. 2009, *ApJ*, 699, 911
- Malkov, M. A. & Drury, L. O. 2001, *Reports on Progress in Physics*, 64, 429
- Massey, P. & Hunter, D. A. 1998, *ApJ*, 493, 180
- Massey, P., Johnson, K. E., & Degioia-Eastwood, K. 1995, *ApJ*, 454, 151
- Melrose, D. B. & Pope, M. H. 1993, *Proceedings of the Astronomical Society of Australia*, 10, 222
- Montmerle, T. 1979, *ApJ*, 231, 95
- Nazé, Y., Antokhin, I. I., Rauw, G., et al. 2004, *A&A*, 418, 841
- Nichols-Bohlin, J. & Fesen, R. A. 1993, *AJ*, 105, 672
- Oey, M. S. & Smedley, S. A. 1998, *AJ*, 116, 1263
- Ohm, S., Horns, D., Reimer, O., et al. 2009, *ArXiv e-prints*
- Parizot, E., Marcowith, A., van der Swaluw, E., Bykov, A. M., & Tatischeff, V. 2004, *A&A*, 424, 747
- Rauw, G., Manfroid, J., Gosset, E., et al. 2007, *A&A*, 463, 981
- Salpeter, E. E. 1955, *ApJ*, 121, 161
- Selman, F., Melnick, J., Bosch, G., & Terlevich, R. 1999, *A&A*, 347, 532
- Smith, N., Egan, M. P., Carey, S., et al. 2000, *ApJ*, 532, L145
- Torres, D. F., Domingo-Santamaría, E., & Romero, G. E. 2004, *ApJ*, 601, L75
- Townsley, L. K., Broos, P. S., Feigelson, E. D., et al. 2006, *AJ*, 131, 2140
- Tsujiimoto, M., Feigelson, E. D., Townsley, L. K., et al. 2007, *ApJ*, 665, 719
- Vladimirov, A., Ellison, D. C., & Bykov, A. 2006, *ApJ*, 652, 1246
- Walborn, N. R. 1991, in *IAU Symposium, Vol. 148, The Magellanic Clouds*, ed. R. Haynes & D. Milne, 145–153
- Walborn, N. R., Drissen, L., Parker, J. W., et al. 1999, *AJ*, 118, 1684
- Walborn, N. R. & Parker, J. W. 1992, *ApJ*, 399, L87
- Wang, Q. & Helfand, D. J. 1991, *ApJ*, 370, 541

depends on the ratio D_u/D_x where D_x is the space diffusion coefficient, controlled by magnetic fluctuations at small scales, and $D_u = UL$ describes the effect of large scale turbulence, where U is the average turbulent speed and L is the average size between turbulence sources.